Microscopic characterisation of suspended graphene grown by chemical vapour deposition

Bignardi, L.; Dorp, W.F. van; Gottardi, S.; Ivashenko, O.; Dudin, P.; Barinov, A.; de Hosson, J.T.M.; Stöhr, M.; Rudolf, P.

Published in:
Nanoscale

DOI:
10.1039/c3nr02386a

Publication date:
2013

Microscopic characterisation of suspended graphene grown by chemical vapour deposition

Luca Bignardi,[a] Willem F. van Dorp,[a] Stefano Gottardi,[a] Oleksii Ivashenko,[a] Pavel Dudin,[†b] Alexei Barinov,[b] Jeff Th. M. de Hosson,[a] Meike Stöhr,[a] and Petra Rudolf[*a]

Received Xth XXXXXXXXXX 20XX, Accepted Xth XXXXXXXXX 20XX
First published on the web Xth XXXXXXXXXX 200X
DOI: 10.1039/b000000x

We present a multi-technique characterisation of graphene grown by chemical vapour deposition (CVD) and thereafter transferred to and suspended on a grid for transmission electron microscopy (TEM). The properties of the electronic band structure are investigated with angle-resolved photoelectron spectromicroscopy, while the structural and crystalline properties are studied with TEM and Raman spectroscopy. We demonstrate that the suspended graphene membrane locally shows electronic properties comparable with those of samples prepared by micromechanical cleaving of graphite. Measurements show that the area over which high quality suspended graphene is obtained is limited by the folding of the graphene during the transfer.

1 Introduction

The growth of graphene on metallic substrates by chemical vapour deposition (CVD) is a well-established technique yielding large graphene flakes[1]. In addition, CVD growth is one of the most promising techniques for production on a large and commercially viable scale[2]. Although CVD-grown graphene generally shows lower electron mobility and more defects than graphene produced by the micromechanical cleaving of graphite[1], the easy transfer from the metal substrate to other substrates gives access to many interesting applications[3–5].

The possibility of using suspended graphene as an ultrathin membrane in electronic devices and sensors has recently lead to intensive investigations, contributing to reveal outstanding electronic[6–10] and interesting mechanical properties, *e.g.* high-mechanical strength[11,12] and micro-filtering qualities[13]. Since the interaction with the substrate can strongly modify the electronic structure of graphene[1], in suspended graphene samples one expects the observation of a Dirac-like dispersion[14] at the Fermi level, which is very close to the theoretically predicted dispersion for self-standing single-layer graphene. Furthermore, suspended graphene is suitable for transmission electron microscopy (TEM) experiments, where stable, thin and strong supporting substrates are necessary, *e.g.* to investigate properties of nanoparticles[11]. A reliable and non-destructive method for transferring graphene from the metal substrate to a TEM grid has been reported[15] but a complete characterisation of these membranes is still lacking.

Herein, we present a study of graphene grown by CVD on copper and subsequently transferred onto TEM grids to produce a suspended layer. Angle-resolved photoemission spectroscopy and microscopy revealed the local electronic structure of this suspended graphene. TEM, electron diffraction and Raman spectroscopy yielded information about the morphology as well as the crystallographic ordering of the suspended areas. These techniques showed that in the suspended areas our samples exhibit single-crystalline domains as well as the electronic structure of non-interacting graphene. In fact, despite the polycrystalline nature of the substrate used for the growth, this graphene exhibits large single-crystalline domains and over the suspended areas the characteristic electronic structure of a non-interacting graphene. We discuss the role and presence of defects and their influence on the photoemission and Raman spectra as well as on the diffraction patterns.

2 Experimental

Graphene was grown on Cu foil (thickness 25 μm, 99.999% purity, ESPI Metals) in a vacuum furnace (base pressure 10^{-5} mbar). The Cu foil was reduced in a mixture of 0.5 mbar of hydrogen (Messer, purity 5.0) and 0.1 mbar of argon (Linde, purity 5.0) for 40 minutes. Afterwards, graphene was grown by exposing the Cu foil to argon (0.1 mbar), hydrogen (0.5 mbar) and methane (0.5 mbar, Messer, purity 4.0) for two min. at a temperature of 1180 K. The sample was subsequently cooled to room temperature in an argon flow

[a] *Zernike Institute for Advanced Materials, University of Groningen, Nijenborgh 4, 9747AG Groningen, The Netherlands.*
[b] *Sinctrotrone Trieste s.c.p.a., 34149 Basovizza, Trieste, Italy.*
[†] *Current address: Diamond Light Source, Harwell Science and Innovation Campus, Didcot, Oxfordshire, OX11 0DE, United Kingdom*

(0.09 mbar) at rate of 15 K/min.

Graphene was then transferred to a TEM holey membrane (Quantifoil® 2/2, EMS), which consists of a 200 Au-mesh square grid, covered by a 12 nm thick amorphous carbon film. This film is patterned with 2 μm circular holes. The TEM membrane was placed directly onto the graphene on Cu foil. A droplet of 2-propanol (Merck, 99.95 % purity) was added on top in order to draw the membrane in close contact with the graphene on Cu foil upon evaporation[15]. The graphene/TEM membrane was then placed in a 5mM solution of $FeCl_3$ in water in order to etch away the copper, leaving the graphene attached to the TEM grid. The TEM grid with the graphene was then rinsed in milliQ water, followed by an annealing in air at 400 K for 5 minutes. A preliminary inspection with scanning electron microscopy showed that the samples consisted of graphene areas which were suspended over 2 μm holes, with a coverage of about 80 % over the entire surface of the sample (not shown).

Angle-resolved photoelectron spectroscopy (ARPES) and ccanning photoemission microscopy (SPEM) were carried out at the SpectroMicroscopy beamline at the ELETTRA Synchrotron, Trieste, Italy, where the impinging photon beam is focused with Schwarzschild optics, resulting in a minimum beam diameter of 600 nm, which makes it suitable for submicrometer imaging and spectroscopy[16]. To remove water and contaminants adsorbed during the transfer in air, the samples were annealed in UHV (base pressure 10^{-10} mbar) for 45 minutes at a temperature of about 570 K prior to the acquisition of photoemission spectra. The experiments were carried out at low temperature (T=100 K) in order to minimize the thermal broadening of the spectra.

The TEM images were collected with a JEOL 2010F TEM operated at 200 keV, which is equipped with a field emission gun. The samples were annealed *in vacuo* before image acquisition at a temperature of about 600 K for 20 min. Imaging was done in bright field mode and diffraction patterns were collected with a camera length of 200 mm. All images were recorded with a Gatan CCD camera. The Raman spectra were acquired with a Olympus BX51 microscope fiber-coupled to an Andor Technology DV420A-BV detector and a 532 nm laser (25 mW, Cobolt Technology). The laser spot size at the sample was ca. 10 μm with a 50x objective.

3 Results and discussion

3.1 Angle-resolved Photoelectron Spectromicroscopy

We acquired a series of large-scale SPEM maps, using a photon beam energy of 27 eV and collecting electrons with a binding energy of 1 eV (referenced to the Fermi level). In figure 1 a 200×150 μm^2 map is shown. Graphene is present in the areas framed with yellow rectangles. The regular pattern of

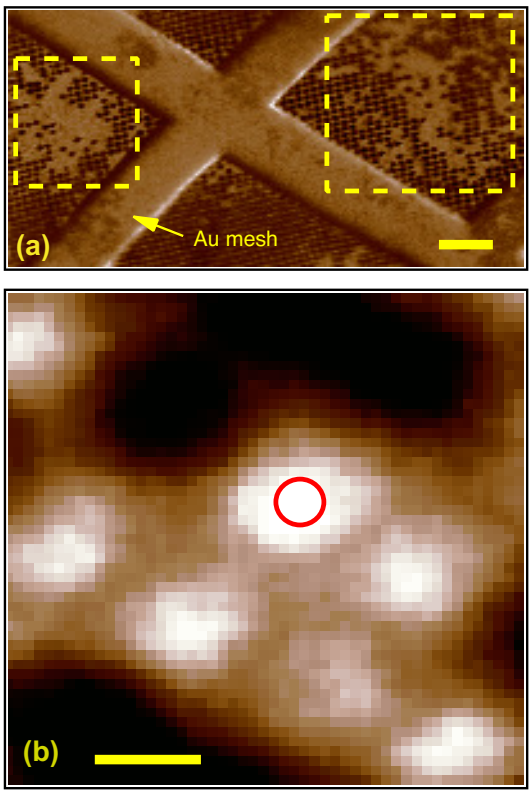

Fig. 1 (a) Scanning photoemission microscopy (SPEM) map, acquired with a photon energy of 27 eV by collecting fast photoelectrons, *i.e.* electrons with a binding energy of 1 eV with respect to the Fermi level. Areas where a suspended graphene layer is present are marked with a dashed yellow frame. The scale bar corresponds to 20 μm. (b) A more detailed SPEM map acquired under the same experimental conditions in the area marked by the dashed yellow frame on the left in panel (a). The red circle indicates the area where ARPES spectra were acquired. The scale bar corresponds to 2 μm. Brighter areas correspond to higher intensity of the photoemission signal.

the holey carbon mesh is not visible there while it is clearly detectable in other areas of the sample. A more detailed map, acquired within the framed area on the left side of figure 1-(a), is presented in figure 1-(b); here an area suitable for acquisition of the band structure of the suspended graphene was identified, as indicated by a red circle.

In panel (a) of figure 2 we report an angle-resolved photoemission spectrum acquired on suspended graphene, with a photon beam energy of 27 eV, spanning the band dispersion along the $\overline{\Gamma K}$ direction of the Brillouin zone of graphene. To enhance the observed features a false colour scale was used, where brighter colour indicates higher photoemission intensity. The zero of the parallel momentum axis was set at the Γ point of the Brillouin zone of graphene. The σ and π bands of the graphene are marked by dashed red and blue lines, respec-

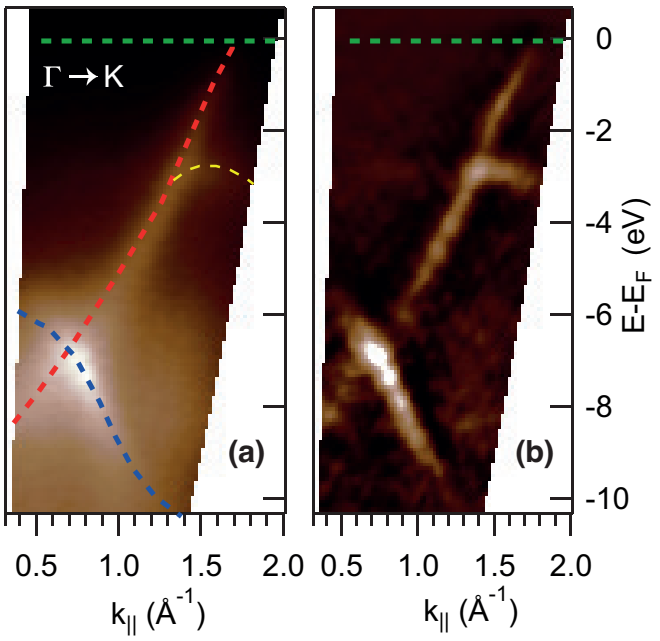

Fig. 2 (a) Band structure of suspended graphene along the $\overline{\Gamma K}$ direction, taken by angle-resolved photoemission spectroscopy. The dashed red and blue lines are a guide to the eye and mark the π and σ bands of graphene respectively, whose shape has been deduced from panel (b). The dashed yellow line marks a branch of π band along the $\overline{\Gamma M}$ direction. The origin of the momentum axis corresponds to the position of the Γ point of graphene. The dashed green line indicates the position of the Fermi level. (b) Same graph as panel (a) after applying a 2D curvature filter to enhance the band structure features.

tively.

By applying a 2D curvature filter[17] to the data presented in figure 2-(a), the band-structure can be enhanced as shown in figure 2-(b). A conical dispersion of graphene π-band centred at the K point of the Brillouin zone can thus be identified. The dispersion looks asymmetric in intensity with respect to the K point: the $\overline{K\Gamma'}$ branch of the cone is not visible. This can be explained by the phase difference of the electrons emitted from A and B sub-lattices, which results in a completely destructive interference, as theoretically predicted[18] and observed in earlier ARPES experiments on graphene[8]. The average Fermi velocity can be obtained from the curvature plot of the bandstructure by extracting the slope of $(E - E_F)$ vs $k_{||}$ in a range of 1 eV below E_F and was found to amount to $v_F = 0.97 \pm 0.08 \times 10^6$ m/s. This value is in the range of values reported for graphene samples produced with micromechanical cleaving and investigated with conductivity measurements[19] or angle-resolved photoemission spectroscopy[8].

A further dispersing band, marked with a dashed yellow line as guide to the eye, is observed in panel (a) of figure 2. Its vertex lies 2.9 eV below the Fermi level, 1.46 Å^{-1} from the Brillouin zone center Γ. The latter value corresponds exactly to the $\overline{\Gamma M}$ distance and thus suggests contributions to the photoemission spectrum from azimuthally rotated domains. In this case, the graphene area under the photon beam comprised domain boundaries which separated domains aligned along $\overline{\Gamma M}$ and $\overline{\Gamma K}$ directions.

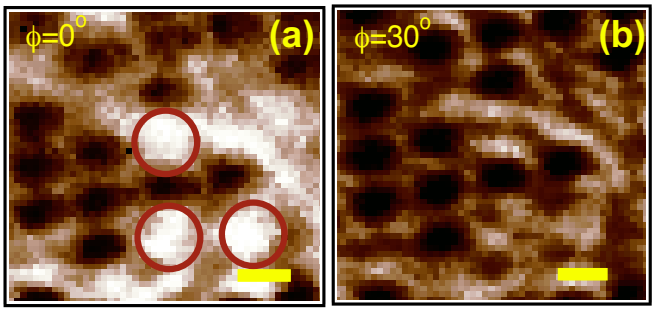

Fig. 3 Scanning photoemission microscopy map, acquired with a photon energy of 27 eV by collecting fast photoelectrons,*i.e.* electrons with a binding energy of 1 eV with respect to the Fermi level at azimuthal angle of 0° (panel (a)) and of 30° (panel (b)). The scale bars correspond to 2 μm. Brighter areas correspond to higher intensity of the photoemission signal. The two images are presented with the same false colour scale and can be directly compared.

More insight into the distribution of the azimuthally rotated domains is obtained from SPEM at different acquisition angles. Figure 3 shows SPEM maps acquired on the same area of the sample but for two different azimuthal angles. Azimuthal angles of 0° and 30° were chosen, because they correspond to the $\overline{\Gamma K}$ and $\overline{\Gamma M}$ high-symmetry directions of the graphene Brillouin zone, respectively. The two images are presented with the same false colour scale and therefore can be directly compared. Corresponding areas show a different photoemission intensity for the two azimuthal angles, which could indicate that there are several crystalline domains in small portions of the sample.

In figure 3-(a) we can identify three holes clearly covered with graphene (marked by red circles), for which the high intensity of the photoemission signal indicates that the azimuthal angle of the analyser matches the $\overline{\Gamma K}$ high-symmetry direction of the Brillouin zone. The image acquired with the analyser directed along the $\overline{\Gamma M}$ direction (30° azimuth) in the figure 3-(b) shows higher intensity at the borders of these holes, indicating that several rotational domains are present in the flakes covering these holes. Furthermore, a higher intensity was also observed in the vicinity of the edges of the graphene flakes for both azimuthal angles. A possible explanation for this may be the contribution from edge states due to the finite size of the graphene layer[20].

3.2 TEM and Raman characterisation

We performed TEM and electron diffraction studies to determine the size and orientation of the crystalline domains of our graphene samples. The TEM micrograph in panel (a) of figure 4 shows a region with suspended graphene. The central and the bottom holes are entirely covered with graphene while the two top holes are only partially covered and there the edges of the graphene sheet are folded over, as indicated by the black arrows. A detailed TEM image of an area with no apparent defects is reported in panel (b) while the corresponding electron diffraction pattern is shown in (c). The single set of hexagonal spots indicates that the graphene membrane is perfectly single-crystalline in this region. Occasionally, as observed on the membrane in the centre of figure 4-(a) and indicated by the white arrow, we could observe nanoparticles containing copper and iron leftovers from the etching procedure*.

A detailed TEM image and an electron diffraction pattern acquired in a defect-rich area close to an edge of the graphene flake are shown in figure 4-(d) and (e) respectively. The diffraction pattern reveals multiple crystalline domains, giving rise to spots arranged along a ring. A systematic study of the TEM images revealed that about 50% of the graphene covered holes exhibited mono-crystalline features, *i.e.* a pattern like that reported in figure 4-(b). We speculate that the diffraction pattern in figure 4-(e) could be the result of differently oriented graphene domains within the same acquisition area and of wrinkles that are forming on the surface, especially in the vicinity of edges.

These results were confirmed by Raman spectroscopy: the size of the laser beam is larger than the areas with suspended graphene; hence the observed spectrum corresponds to a spatial average over areas with suspended and with supported graphene. In figure 5 we report the spectrum acquired on the graphene-covered TEM grid (continous blue line) and on the bare TEM grid (dashed grey line). The prominent peak observed at a shift of 1583 cm^{-1} for the graphene-covered TEM grid corresponds to the G-band, while the peaks at 1358 cm^{-1} and at 2680 cm^{-1} are the D and G' bands of graphene, respectively[21]. The relative intensity and positions of these peaks were homogeneous on the entire sample surface. The G' peak could be fitted with a single Lorentzian (FWHM 51.5$\pm$1.5 cm^{-1}), confirming that the membrane was composed of single-layer graphene[21]. The G peak displayed a shoulder toward lower wavenumbers and did not appear to be as sharp as for graphene obtained by micromechanical cleaving[22]. This might be due to graphene which is locally folded over, as observed in the TEM image discussed above. This hypothesis is supported by the fact that a similar shape of the G peak was observed in single-walled carbon nanotubes[23], where the graphene sheet is strongly curved. The presence of a shoulder of the D peak towards lower wavenumbers is in agreement with what was reported for spectra of edges of graphite and graphene[21,24]. The bands centerd at 1100, 800 and 600 cm^{-1} are also observed for the TEM grid without the graphene layer and therefore attributed to amorphous carbon[25].

In conclusion we presented a multi-technique characterisa-

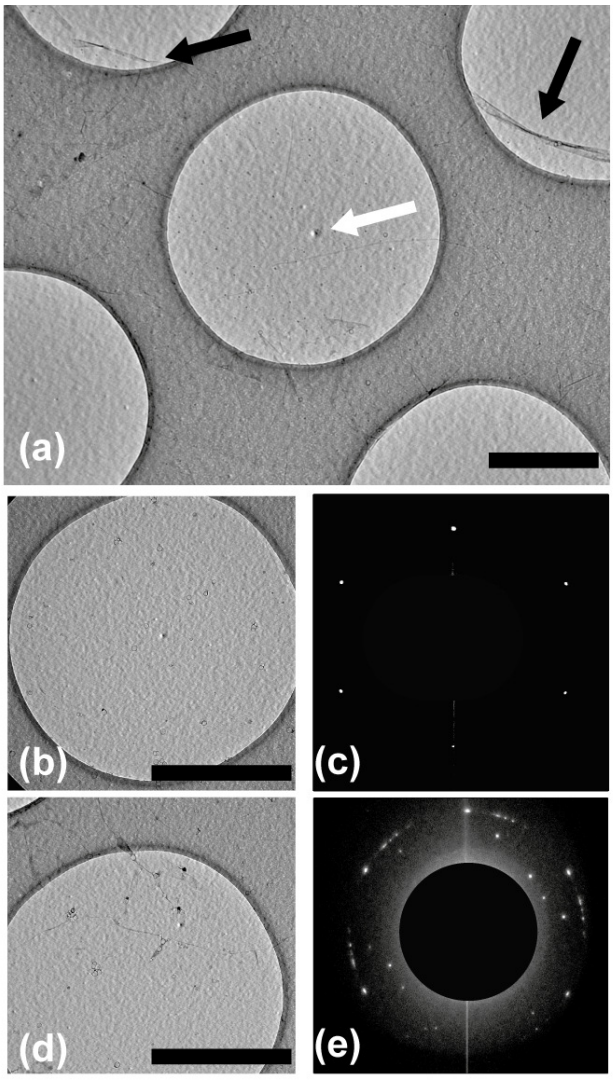

Fig. 4 (a) TEM micrograph of a suspended graphene sample. The magnification is 30kx. The black arrows point to areas where the graphene membrane is folded over itself, at the edges of a flake. The scale bar is 1 μm. (b) Detailed image of a single-crystalline area. (c) Electron diffraction pattern acquired on the area shown in panel (b). (d) Detailed image of a defect-rich area. (e) Electron diffraction pattern acquired on the area shown in panel (d). The non-diffracted beam is masked to enhance the contrast of the diffraction pattern.

* The nature of the nano particles was determined by Energy-dispersive X-ray spectroscopy.

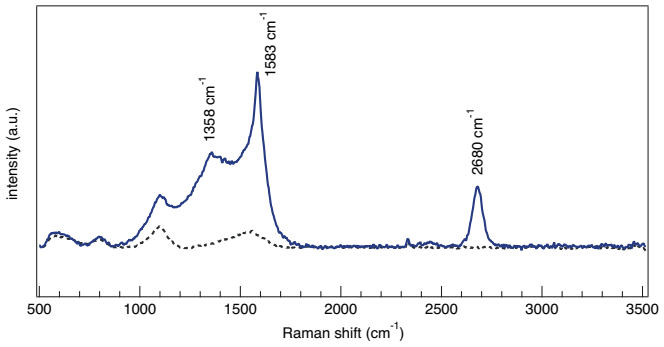

Fig. 5 Raman spectrum (blue line) acquired on graphene covering a holey TEM membrane. The laser spot covered suspended as well as supported graphene areas. The spectrum acquired on the bare holey TEM membrane is also shown (dashed grey line). The low intensity band at about 2300 cm^{-1} is an artefact of the detector.

tion of the local electronic and structural properties of CVD-grown graphene, suspended on TEM grids. The investigated samples displayed electronic properties similar to free-standing graphene produced by micromechanical cleaving, with a Fermi velocity close to the theoretical value. Furthermore our method of CVD growth and stamp-free transfer to the TEM grid was shown to yield suspended graphene membrane areas which in 50% of the cases were single-crystalline over the entire area of each hole in the TEM grid. We speculate that the wrinkles and the curvature of the graphene at the edges of the flake, revealed by TEM, could be the only features that limit the quality in view of a possible future use as ultrathin TEM membranes and in large-scale electronics.

This work was supported by the Foundation for Fundamental Research on Matter (FOM), part of the Netherlands Organisation for Scientific Research (NWO) and by the European Research Council (ERC-2012-StG 307760-SURFPRO). W.F.v.D acknowledges a VENI grant, id 10684, from the Netherlands Organization for Research (NWO), made possible by the Foundation for Technical Sciences (STW). The authors thank Bart J. van Wees for the use of the Raman equipment and Luc Venema for technical support.

References

1 M. Batzill, *Surface Science Reports*, 2012, **67**, 83.
2 M. J. Allen, V. C. Tung and R. B. Kaner, *Chemical Reviews*, 2010, **110**, 132.
3 C. Mattevi, H. Kim and M. Chhowalla, *Journal of Materials Chemistry*, 2011, **21**, 3324.
4 X. Li, W. Cai, J. An, S. Kim, J. Nah, D. Yang, R. Piner, A. Velamakanni, I. Jung, E. Tutuc, S. K. Banerjee, L. Colombo and R. S. Ruoff, *Science*, 2009, **324**, 1312.
5 X. Li, W. Cai, L. Colombo and R. S. Ruoff, *Nanoletters*, 2009, **9**, 4268.
6 J. C. Meyer, A. K. Geim, M. I. Katsnelson, K. S. Novoselov, T. J. Booth and S. Roth, *Nature*, 2007, **446**, 60.
7 K. Bolotin, K. Sikes, Z. Jiang, M. Klima, G. Fudenberg, J. Hone, P. Kim and H. Stormer, *Solid State Communications*, 2008, **146**, 351.
8 K. R. Knox, A. Locatelli, M. B. Yilmaz, D. Cvetko, T. O. Mentes, M. A. Niño, P. Kim, A. Morgante and R. M. O. Jr., *Physical Review B*, 2011, **84**, 115401.
9 R. Zan, C. Muryn, U. Bangert, P. Mattocks, P. Wincott, D. Vaughan, X. Li, L. Colombo, R. S. Ruoff, B. Hamilton and K. S. Novoselov, *Nanoscale*, 2012, **4**, 3065.
10 C. N. Lau, W. Bao and J. V. Jr, *Materials Today*, 2012, **15**, 238.
11 C. Lee, X. Wei, J. W. Kysar and J. Hone, *Science*, 2008, **321**, 385.
12 I. W. Frank, D. M. Tanenbaum, A. M. van der Zande and P. L. McEuen, *Journal of Vacuum Science and Technology B*, 2007, **25**, 2558.
13 J. Bunch, S. Verbridge, J. Alden, A. Van Der Zande, J. Parpia, H. Craighead and P. McEuen, *Nano Letters*, 2008, **8**, 2458.
14 A. H. Castro Neto, F. Guinea, N. M. R. Peres, K. S. Novoselov and A. K. Geim, *Rev. Mod. Phys.*, 2009, **81**, 109.
15 W. Regan, N. Alem, B. Alemán, B. Geng, Ç. Girit, L. Maserati, F. Wang, M. Crommie and A. Zettl, *Applied Physics Letters*, 2010, **96**, 113102.
16 P. Dudin, P. Lacovig, C. Fava, E. Nicolini, A. Bianco, G. Cautero and A. Barinov, *Journal of Synchrotron Radiation*, 2010, **17**, 445.
17 P. Zhang, P. Richard, T. Qian, Y.-M. Xu, X. Dai and H. Ding, *Review of Scientific Instruments*, 2011, **82**, 043712.
18 E. L. Shirley, L. J. Terminello, A. Santoni and F. J. Himpsel, *Physical Review B*, 1995, **51**, 13614.
19 D. C. Elias, R. V. Gorbachev, A. S. Mayorov, S. V. Morozov, P. Zhukov, A. A. Blake, L. A. Ponomarenko, I. V. Grigorieva, K. S. Novoselov, F. Guinea and A. K. Geim, *Nature Physics*, 2011, **7**, 701.
20 K. Nakada, M. Fujita, G. Dresselhaus and M. S. Dresselhaus, *Phys. Rev. B*, 1996, **54**, 17954.
21 L. M. Malard, M. A. Pimenta, G. Dresselhaus and M. S. Dresselhaus, *Physics Reports*, 2009, **473**, 51.
22 A. C. Ferrari, J. C. Meyer, V. Scardaci, C. Casiraghi, M. Lazzeri, F. Mauri, S. Piscanec, D. Jiang, K. S. Novoselov, S. Roth and A. K. Geim, *Phys. Rev. Lett.*, 2006, **97**, 187401.
23 M. S. Dresselhaus, A. Jorio, M. Hofmann, G. Dresselhaus and R. Saito, *Nano Letters*, 2010, **10**, 751.
24 L. G. Cançado, M. A. Pimenta, B. R. A. Neves, M. S. S. Dantas and A. Jorio, *Phys. Rev. Lett.*, 2004, **93**, 247401.
25 A. C. Ferrari and J. Robertson, *Philosophical Transactions of the Royal Society of London. Series A: Mathematical, Physical and Engineering Sciences*, 2004, **362**, 2477.